Accepted Manuscript

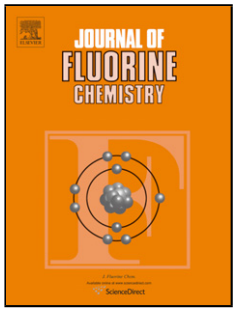

Title: Effect of fluoride-mediated transformations on electrocatalytic performance of thermally treated TiO_2 nanotubular layers

Authors: Hanna Maltanava, Sergey Poznyak, Maria Ivanovskaya, Nico Scharnagl, Maksim Starykevich, Andrei N. Salak, Maria de Rosário Soares, Alexander Mazanik

PII: S0022-1139(18)30500-1
DOI: https://doi.org/10.1016/j.jfluchem.2019.02.006
Reference: FLUOR 9289

To appear in: *FLUOR*

Received date: 14 December 2018
Revised date: 12 February 2019
Accepted date: 13 February 2019

Please cite this article as: Maltanava H, Poznyak S, Ivanovskaya M, Scharnagl N, Starykevich M, Salak AN, de Rosário Soares M, Mazanik A, Effect of fluoride-mediated transformations on electrocatalytic performance of thermally treated TiO_2 nanotubular layers, *Journal of Fluorine Chemistry* (2019), https://doi.org/10.1016/j.jfluchem.2019.02.006

Effect of fluoride-mediated transformations on electrocatalytic performance of thermally treated TiO_2 nanotubular layers

Hanna Maltanava[a], *Sergey Poznyak*[a*], *Maria Ivanovskaya*[a], *Nico Scharnagl*[b], *Maksim Starykevich*[c], *Andrei N. Salak*[c], *Maria de Rosário Soares*[d], *Alexander Mazanik*[f]

[a]Research Institute for Physical Chemical Problems, Belarusian State University, Leningradskaya Str. 14, 220006 Minsk, Belarus

[b]Helmholtz-Zentrum Geesthacht Centre for Materials and Coastal Research GmbH, Max-Planck-Straße 1, 21502 Geesthacht, Germany

[c]Department of Materials and Ceramics Engineering, CICECO-Aveiro Institute of Materials, The University of Aveiro, 3810-193 Aveiro, Portugal

[d]Central Analytical Laboratory, CICECO-Aveiro Institute of Materials, University of Aveiro, 3810-193 Aveiro, Portugal

[f]Belarusian State University, Nezalezhnastsi Av. 4, 220030 Minsk, Belarus

[*]E-mail: poznyak@bsu.by

Graphical Abstract

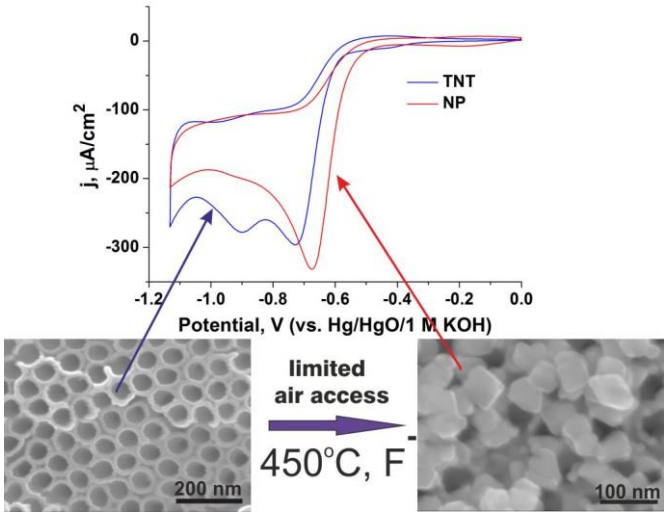

Highlights

- Fluoride-mediated transformation of TiO_2 nanotubes into TiO_2 nanoparticles during their annealing in a confined space
- Morphology, crystalline structure and chemical composition of TiO_2 nanotubes and TiO_2 nanoparticles were compared
- Fluorine doping has a positive effect on electrocatalytic performance of TiO_2 nanoparticles in oxygen reduction reaction

ABSTRACT:

The peculiarities of morphology, crystalline structure and chemical composition of TiO_2 nanotubular layers (TNT) and TiO_2 nanoparticulate (NP) layers obtained by fluoride-mediated transformation of TNT have been described in the present paper. The annealing of amorphous TNT in a confined space under limited air access conditions leads to TNT-to-NP transformation accompanied by fluorine doping of the titania matrix as supported by X-ray photoelectron spectroscopy investigations. The collapse of tubular structure as well as the formation of nanoparticles was confirmed using scanning electron microscopy (SEM), X-ray diffraction (XRD) and Raman spectroscopy. Electrocatalytic activity of both TNT and NP electrodes toward oxygen reduction reaction (ORR) has been examined by cyclic voltammetry (CV). The positive shift of ORR wave of the NP layers in comparison with TNT makes the NP-based electrodes

more suitable for oxygen reduction. The improved activity of the NP electrodes is attributed to the increased concentration of redox active Ti^{3+} species owing to fluorine doping of TiO_2 which plays a crucial role in electroreduction of oxygen molecules.

KEYWORDS: Titanium dioxide, Fluorine doping; Nanotubes, Nanoparticles, Electrocatalysis, Oxygen reduction reaction

1. INTRODUCTION

Recently, nanostructured titanium dioxide has attracted considerable scientific interest due to combination of specific properties (unique optical properties, high catalytic activity, large surface area and unusual mechanical characteristics) in comparison to the bulk TiO_2 which makes this material useful for large-scale potential applications such as solar cells, water splitting for hydrogen generation, battery cathode materials, sensors, recording materials and others [1−6]. It is generally accepted that structural and morphological features have a big impact on the performance of TiO_2 nanomaterials. In nature, TiO_2 occurs in three different polymorphs: anatase, rutile and brookite [7]. Rutile is widely used as a white pigment, while anatase is the most active polymorph in photocatalysis [8, 9]. As for brookite, it remains to be the least studied phase, mainly owing to the difficulties with obtaining its pure phase [10]. It should be noted that not only anatase and rutile demonstrate varying photoactivity, but the different crystallographic orientations of the same TiO_2 polymorph may exhibit different activities [11]. In particular, both theoretical and experimental studies have demonstrated that the surface of [001] facets of anatase exhibits a very high reactivity [12]. Moreover, incorporation of different dopants (N, C, S, F), along with Ti^{3+} formation, H^+ uptake *etc.*, can introduce additional energy states in the oxide band gap, thus resulting in modification of electronic and optical properties of TiO_2 [2, 13−18].

Interest in nanostructured titania has extended by development of 1D structures including nanotubes, nanorods, nanowires and nanofibers [19]. Among nanostructured TiO_2 materials, highly ordered TiO_2 nanotubes (TNT) are the most interesting structures owing to the possibility of efficient 1D charge transport, enhanced light absorption and propagation characteristics arising from their precisely controlled and oriented porosity, and excellent performance in alkali and acidic environment [20]. Therefore, particular attention was given to the preparation of titania nanotubes and many methods were developed, including the hydro/solvothermal treatment of TiO_2 nanoparticles with an alkaline solution, anodization of Ti foil, template-assisted methods and others [21−23]. Nowadays, electrochemical anodization of titanium in

fluoride-containing electrolytes is considered to be the most simple and prevalent approach for titania nanotubular layer production [2, 24−26]. Significant efforts were made to optimize anodization conditions for preparing TNT layers of desirable morphology and thickness [6, 27−29]. Over the past few years, the third generation of TNT has attracted particular interest, where introduction of organic electrolytes such as ethylene glycol and glycerol with a small amount of water and F^- ions allows the formation of highly ordered, smooth, uniformly shaped and significantly long tubes [27, 30]. It is well-known that as-formed TNT layers are amorphous, but *via* annealing they can be converted to the crystalline forms of anatase or rutile [31]. Interestingly, the annealing conditions can be crucial for reservation of tubular structure as well as for doping of TNT through thermal treatment in different gas atmosphere [32−36]. Recently, Alivov and Fan have reported on the transformation of TNT into nanoparticles (NP) under controllable annealing conditions [37, 38]. Necessary parameters for such transformation are the high temperature raping rate and the close contact of TNT's open end with a supporting glass slide which needs for catalytic reaction of fluoride residues in TNT with TiO_2. Such nanotube-to-nanoparticle transition upon annealing in fluorine ambient can certainly alter the physical-chemical properties of the TiO_2 material. For example, the formation of TiO_2 nanoparticles in the presence of fluoride ions can be accompanied by the increase of surface area with a high portion of reactive [001] facets [39]. At the same time, the electron lifetime and charge collection efficiency can be decreased significantly for nanoparticulate layers as compared to nanotubular ones [40]. Thus, the monitoring of TNT-to-NP transformation is an important issue to predict the behavior of resultant material and to fabricate the nanostructured TiO_2 electrodes with desired properties. Moreover, the presence of fluorine atoms could also determine the properties of the TiO_2 surface in catalysis, gas sensing, *etc.* [41−43].

Recently, nanostructured TiO_2 electrodes including nanotubes have received attention as a potential support for active metallic catalysts in fuel cells [44−48]. Besides, Sacco et al. [49] have shown that TNT layers can be considered as promising electrocatalytic material itself, since catalytic performance of the crystalline TNT in oxygen reduction reaction (ORR) is only slightly lower with respect to platinum. This fact dictates the necessity of detailed investigation of electrocatalytic activity of bare TNT as well as NP layers obtained via TNT-to-NP transformation.

In the present work we provide direct comparison of morphology, crystalline structure and chemical composition of titania nanotubes and nanoparticulate layers formed as the result of fluoride-mediated TNT-to-NP transformation during thermal treatment in a confined space under limited air access conditions. Scanning electron microscopy (SEM), powder X-ray diffraction (XRD), X-ray photoelectron spectroscopy (XPS) and Raman spectroscopy were used for

characterization of the obtained nanostructures. Furthermore, electrocatalytic activity of both TNT and NP electrodes in oxygen reduction reaction was studied and discussed.

2. EXPERIMENTAL

Self-organized highly ordered titania nanotubular layers were produced on commercially pure titanium sheets (4 cm × 1 cm; 99.7 % Ti, Alfa Aesar) by two-steps anodization in ethylene glycol electrolyte containing 0.75 wt% NH_4F and 2 vol. % H_2O. The Ti sheets were polished mechanically and then chemically in a HF:HNO_3 (1:2 by volume) mixture to mirror finish and finally rinsed with deionized water. The anodizing cell has a two electrode configuration with a Pt sheet as the cathode and the Ti sheet as the anode. The electrochemical anodization for both steps consisted of a potential ramp from 0 to 40 V (sweep rate - 200 mV s^{-1}) followed by holding the potential constant for 1 h. The oxide film formed during the first step of anodization was removed by detachment in an ultrasound bath with deionized water. Before the second anodization, the electrochemical cell was filled with a fresh portion of the electrolyte. After the second step of anodization, the samples were washed with ethanol and then their surface was cleaned from debris by treatment in an ultrasound bath with distilled water during 30 s. One part of the anodized samples was used to produce crystalline TNT layers, other part was taken to convert amorphous TNT layers to the NP ones. In order to obtain crystalline TiO_2, the samples were annealed at 450 °C for 3 h (heating rate – 5 °C/min) using a tube furnace (TERMOLAB-Fornos Eléctricos, Lda.). To ensure a formation of well-defined tubular structure, the thermal treatment was performed in air flow (ALPHAGAZ^{TM} 1 AIR, O_2 concentration – 20±1%). Under such conditions, NH_4F and other fluorine-containing species, which inevitably remain in the amorphous TNT layers even after washing, are dragged by the flow without reacting with titania. On contrary, when the thermal treatment occurs in conditions of a restricted mass transfer, the fluorides react with the amorphous TNT matrix that results in destruction of the nanotubes and formation of nanoparticles. Therefore, an annealing of the samples aimed at the TNT-to-NP transformation was carried out at limited air access in a narrow long quartz tube with a sealed end (the samples were placed near the sealed end) or by covering up them with a glass slide resulted in the transformation of nanotubes into nanoparticles.

Microstructure and surface morphology of the samples were characterized using using a Hitachi SU-70 and a Hitachi S-4800 scanning electron microscopes, as well as a Hitachi H-800 transmission electron microscope (200 kV). Phase identification was performed using a PANalytical Empyrean diffractometer (Ni-filtered Cu Kα radiation, step 0.02°, 2-s exposition per step over the angular range of 10-80°). The crystallite orientation study was carried out using a PANalytical X'Pert PRO MRD high-resolution 4-circle diffractometer in Cu K_α radiation.

Position of the detector was fixed at the reflection angle corresponding to diffraction from the (004) plane. Pole densities were plotted in stereographic projection with the plane of the projection chosen to be parallel to the sample surface. Raman spectroscopy was also applied to compare the crystallite orientations in the samples. Raman spectra were taken at room temperature using a Nanofinder HE (Lotis TII, Belarus–Japan) confocal microscope based setup. Raman scattering was excited using the 532-nm solid-state laser (0.6 mW, 120 s). X-ray photoelectron spectroscopy (XPS) was used to analyze the influence of different annealing conditions on chemical composition and electronic state of elements in the specimens. XPS analysis was performed on a Kratos DLD Ultra spectrometer using Al Kα monochromatized radiation (E=1486.6 eV). For survey spectra, pass energy (PE) of 160 eV was used while for regions PE was 20 eV. XPS spectra were recorded before and after Ar^+ etching at different sputtering time (sputter rate 8 nm/min calibrated on Ta_2O_5). All the binding energies (BEs) were referenced to the C 1s peak at 284.8 eV of the surface adventitious carbon.

The electrocatalytic activity of both TNT and NP electrodes in oxygen reduction reaction was examined by cyclic voltammetry (CV) using an Autolab PGSTAT 302N potentiostat in a 0.1 M KOH solution saturated with oxygen during 1 h. Electrochemical experiments were performed in a single-compartment glass cell using a standard three-electrode configuration. An Hg/HgO electrode filled with 1 M KOH (Radiometer Analytical) and a Pt foil were used as the reference and counter electrodes, respectively. The potential sweep rate was 10 mV s^{-1}.

3. RESULTS AND DISCUSSION

3.1 Microstructure characterization

Figure 1a shows typical SEM images of the as-grown TNT layer obtained by two-steps anodization in ethylene glycol based electrolyte. Well-defined tubular structure with a relatively narrow distribution of the inner pore diameter (60±5 nm) and the wall thickness (12±2 nm) can be observed. After the thermal treatment in the air flow, the TNT sample has grey color and preserves the ordered tubular structure (Fig. 1b). The cross-sectional view also demonstrates the well-aligned nanotubular arrays of 10±1 μm length (Fig. 1c).

The as-grown titania layers annealed under limited air access were found to become of whitish colour and to transform into nanoparticular layers (Fig. 2a-c). The thickness of such layers was appr. 6 μm (Fig. 2c). The observed decrease in the thickness of the NP layers in comparison with the TNT ones can be explained by disturbance of the tubular architecture due to nanotube collapse and recrystallization into bigger nanoparticles. The average size of the formed

nanoparticles was estimated to be ~50 nm (Fig. 2a). Meanwhile, larger particles (150−200 nm) and broken parts of the nanotubes were also observed in some areas of the sample (Fig. 2b).

TEM analysis additionally confirmed the TNT-to-NP transformation of titania matrix under limited air access. The tubular morphology was observed for the TNT sample annealed in air flow (Fig. 1d). For the NP sample, nanotubular morphology partially disappeared to form the nanoparticles (Fig. 2d).

3.2 XRD analysis and the crystallite orientation study

XRD analysis showed that the as-grown TNT layers are expectedly amorphous. The XRD patterns of the annealed TNT and NP layers indicate a single-phase anatase crystalline form in both samples (Figure 3). The NP layer demonstrates the diffraction pattern with the angular positions and the relative intensities of the diffraction peaks typical of a standard polycrystalline anatase (JCPDS card No 84−1286), with the (101) reflection as the strongest peak. The average crystallite size in the NP sample calculated based on the integral breadth values of the diffraction peaks (200) and (004) using the Scherrer equation was about 55 nm that is a good agreement with the SEM observations (Figure 2). The XRD pattern of the TNT sample indicates a preferred orientation of crystallites in the [001] direction perpendicular to the substrate. As compared to the NP sample, the (004) peak of the TNT layer is significantly higher (the strongest), whereas the (101) and (200) peaks are considerably lower. The [001] texture coefficient of the TNT sample evaluated by Harris method [50, 51] is 3.4, that demonstrates a strong preferred orientation of TiO_2 crystallites in this crystallographic direction.

3.3 Raman spectroscopy study

The anatase phase of the TNT and NP samples was clearly identified by Raman spectroscopy. Both samples exhibit typical Raman bands (see Fig. 4) at 635 cm^{-1} (E_g vibration mode), 514 cm^{-1} (A_{1g} mode), 396 cm^{-1} (B_{1g} mode) and 198 cm^{-1} (E_g mode) as well as intensive band at 144 cm^{-1} (E_g mode) which are characteristic of anatase phase [52]. However, the relative intensities of the Raman bands are different for the TNT and NP layers. The NP sample has a Raman spectrum similar to the standard anatase polycrystalline materials. In case of the TNT sample, intensities of the bands at 396 cm^{-1} (B_{1g} mode) and 514 cm^{-1} (A_{1g} mode) are enhanced in comparison with the NP sample. According to the literature data [53], the percentage of anatase [001] exposed facets can be determined from the peak intensity ratio of the E_g and A_{1g} modes. We estimated this parameter using the E_g peak at 144 cm^{-1} and the A_{1g} peak at 514 cm^{-1} and found that percent of the [001] facets oriented parallel to the film surface is significantly higher for TNT layers (19 %) as compared with NP ones (5 %).

3.4 XPS spectra and chemical composition

Chemical composition of the TNT and NP layers has been studied by XPS method. The layers were found to consist of titanium (Ti 2p), oxygen (O 1s), carbon (C 1s), fluorine (F 1s) and a negligible amount of nitrogen (N 1s). The Ti/O molar ratio for both samples before Ar^+ etching was approximately 1:3 due to the presence of surface hydroxyl groups and probably some organic contaminants. After etching with Ar^+ ions the Ti/O ratio becomes close to the expected stoichiometric value (1:2). Figure 5 demonstrates the high-resolution XPS spectra of the Ti 2p level for TNT and NP samples before Ar^+ etching. The Ti 2p (3/2) and 2p (1/2) peaks were centered at 458.8 and 464.5 eV, respectively, in accordance with literature data for octahedrally coordinated Ti^{4+} in TiO_2 [54−56]. Additional XPS peak with a lower binding energy of 457.4 eV (fitting curve in blue) is assigned to Ti^{3+} states [57, 58]. The area ratio of Ti^{3+} to Ti^{4+} 2p (1/2) peaks is higher for the NP sample, indicating a larger Ti^{3+} state density in the NP sample in comparison with TNT one. The O 1s peaks located at 530.1 eV and 531.7 eV are assigned to lattice oxygen in TiO_2 and hydroxyl groups (Ti-OH), respectively [54−56, 59, 60].

Figure 6 shows the high-resolution XPS spectra of the F 1s region. An analysis of this region for TNT and NP samples before and after Ar^+ etching allows identifying significant difference in fluorine content and contribution of different fluorine states. Before the etching, only one symmetrical F 1s peak at 685.3 eV was revealed for both TNT and NP samples. The F 1s XPS spectrum of the TNT layer was not markedly changed after etching. The only difference was detected in the relative area of the F 1s peak: it dropped significantly (the atomic concentration of fluorine decreases from 0.9 at.% to 0.25 at.%). In contrast, the spectrum of the NP sample after etching was clearly composed of two contributions: a main peak at 685.3 eV and a smaller peak at 687.1 eV. The main peak located at 685.3 eV can be assigned to the surface fluoride formed by ligand exchange between F^- and surface hydroxyl groups on TiO_2 [61−63] or to F atoms of $TiOF_2$ [41, 64]. The peak at higher binding energy (687.1 eV) can be attributed to substitutional F atoms in the TiO_2 lattice [41, 60, 61, 64]. The atomic concentration of fluorine in the NP sample before and after Ar^+ etching was 0.8 at.% and 2 at.%, respectively. Additionally conducted EDS mapping revealed homogeneous distribution of fluorine on the surface of the TNT and NP layers.

It is worth mentioning that the fluorine concentration after Ar^+ etching was reduced by a factor of 3.6 for the TNT samples and increased by a factor of 2.5 for the NP ones. The enhanced concentration of F^- ions in the depth of the NP layer relative to the surface and the presence of additional chemical state of fluorine (687.1 eV) are the evidence of fluoride ions interaction with TiO_2 which results in the collapse of nanotubular architecture and its transformation to randomly packed nanoparticles. Probably during thermal treatment under conditions of a restricted mass

transfer, both NH_4F and the products of its decomposition (for example, HF) react with amorphous TiO_2, producing complex species such as TiF_6^{2-} [65]. Then, thermal decomposition of these complexes can give crystalline TiO_2 nanoparticles.

3.5 Cyclic voltammetry measurements in Ar-saturated solutions

Electronic properties of the TNT and NP electrodes in the absence of faradaic processes were studied by cyclic voltammetry in deoxygenated alkaline solution. Figure 7 shows the cyclic voltammograms (CVs) of the electrodes in an Ar-saturated 0.1 M KOH electrolyte. At potentials less than ca. -0.9 V an exponential rise of the cathodic current is observed. This electrochemical process can be related to electron accumulation within TiO_2 film coupled to proton uptake from electrolyte for charge compensation. As a result, electrochemical reductive doping of the TiO_2 electrodes takes place. This reaction is reversible and an anodic current is registered when the potential is scanned in the positive direction.

Apart from the currents at E < -0.9 V, a pair of cathodic peak and related significantly broader anodic one is observed at CVs in the range from -0.4 to -0.9 V for both TNT and NP electrodes. The observed peaks are characteristic of nanostructured titania electrodes and can be attributed to filling/depopulation of deep traps located at grain boundaries [66]. Figures 8a and 8b show cyclic voltammograms of TNT and NP electrodes recorded in an Ar-saturated 0.1 M KOH solution at various scan rates in the range up to -0.9 V. The potential of the cathodic peak is slightly shifted in the negative direction when the scan rate increases. As shown in Figures 8c and 8d, the cathodic peak current varies linearly with scan rate, indicating that there are no diffusion limitations for this process. We estimated the charge (Q_{tr}) corresponding to the cathodic peak and found that its value varies insignificantly with the scan rate and is close to the charge of the coupled broad anodic peak. It is significant that the cathodic peak assigned to deep traps is essentially higher for NP electrodes than for TNT ones. The value of Q_{tr} is $(1.2 \div 1.3) \times 10^{-4}$ C cm^{-2} for TNT and $(4.6 \div 4.9) \times 10^{-4}$ C cm^{-2} for NP. Moreover, the position of this peak for NP is shifted by ca. 200 mV in the negative direction as compared with TNT. These results indicate that the energetic position of deep traps in the TiO_2 band gap is markedly changed and their density increases when the nanotubes are transformed into nanoparticles.

3.5 Oxygen electroreduction reaction on TNT and NP electrodes

The effect of the fluoride-mediated TNT-to-NP transformation and related fluorine doping of TiO_2 on its electrocatalytic activity was studied on an example of oxygen electroreduction

reaction, since this process is very important in various applications. Figure 9 displays the CV curves recorded in oxygen-saturated alkaline solution for both TNT and NP electrodes. The voltammetric response of the TNT is characterized by two well defined waves at potentials more negative than -0.7 V. It is noteworthy that the second wave of cathodic current at -0.9 V (vs. Hg/HgO/1M KOH) was revealed only for highly ordered titania nanotubular layers [47, 49] and is not typical for other compact polycrystalline films [67, 68] and single crystals of TiO_2 [69]. The origin of the second wave of oxygen electroreduction on the TNT electrodes is still not clear and requires additional investigation. Characteristically this wave almost disappears after transformation of the TNT layers to the NP ones (Fig. 9).

As seen from Figure 9, the half-wave potential of the oxygen reduction reaction on the NP electrodes shows a well reproducible positive shift by appr. 50 mV in comparison with the TNT layers, signifying the advantage of NP over TNT as the electrocatalyst in ORR. The enhanced ORR activity on the NP electrodes can be related to the destruction of tubular structure accompanied by fluorine doping of the TiO_2 matrix. It was previously reported [67, 68, 70] that oxygen reduction on titania proceeds through the interaction of oxygen (chemical adsorption and dissociative activation of oxygen molecules) with surface defective Ti species. This chemical stage precedes the interfacial charge transfer step. In a number of works devoted to oxygen electroreduction reaction the authors suggested that the surface Ti^{3+} species can be considered as active sites which can mediate the ORR at TiO_2 [67, 68, 70, 71]. For this reason the number and activity of these redox centers could be important factors to define the overall catalytic performance of TiO_2 electrodes. Introduction of F^- ions in the O^{2-} sites of the titania lattice needs one additional electron for charge compensation. This electron localizing on a lattice cation provokes its reduction from Ti^{4+} to Ti^{3+}. The formation of Ti^{3+} species as a result of fluorine insertion in the TiO_2 structure was previously supported by theoretical calculations and ESR measurements [62]. This additional Ti^{3+} generation owing to F^- doping of the TiO_2 structure can lead to enhancing ORR activity and, as a result, to a decrease of the ORR overpotential for NP electrodes.

The CV measurements at the TiO_2 electrodes in deaerated electrolytes demonstrate that some surface species are involved in a reversible electron transfer in the same potential region where the irreversible electroreduction of O_2 takes place (Figs. 8 and 9). The concentration of these species increases significantly after transformation of nanotubes to nanoparticles. We can suggest that these species mediate the electroreduction of oxygen on the titania surface.

CONCLUSION

Titania nanoparticulate layers were synthesized through fluorine-mediated transformation of anodically-grown TiO_2 ordered nanotubular layers during their annealing in a confined space at limited air access. This transformation is confirmed by SEM observations and occurs due to reaction of titania with fluorides remaining in the nanotubular layers from the electrolyte. XRD and Raman spectroscopy measurements showed both annealed nanotubular and nanoparticulate samples to consist of pure anatase phase with a pronounced preferred orientation of crystallites in the [001] direction for nanotubular layers and without any preferred orientation for nanoparticulate ones. XPS analysis indicated that the nanotubes-to-nanoparticles transformation is accompanied by incorporation of fluorine into the TiO_2 lattice. The fluorine doping was found to have a positive effect on electrocatalytic performance of the titania electrodes in oxygen reduction reaction. The overpotential of ORR decreases by appr. 50 mV after nanotubes-to-nanoparticles transformation. Additional generation of Ti^{3+} active centers owing to fluorine doping of titania was suggested to be responsible for improved electrocatalytic activity of the nanoparticulate electrodes.

ACKNOWLEDGMENT

We acknowledge funding from SMARCOAT project. This project has received funding from the European Union's Horizon 2020 research and innovation programme under the Marie Skłodowska-Curie grant agreement No 645662. We thank Dr. M. Makhavikou (A.N. Sevchenko Institute of Applied Physical Problems, Belarusian State University) for carrying out the TEM experiments, as well as employees of the scientific-technical center "Belmicrosystems" of JSC "Integral" for the SEM studies.

REFERENCES

[1] P. V. Kamat, TiO_2 nanostructures: Recent physical chemistry advances, J. Phys. Chem. C. 116 (2012) 11849–11851. doi:10.1021/jp305026h.

[2] P. Roy, S. Berger, P. Schmuki, TiO_2 nanotubes: synthesis and applications, Angew. Chem. Int. Ed. 50 (2011) 2904–2939. doi:10.1002/anie.201001374.

[3] D. Regonini, C.R. Bowen, A. Jaroenworaluck, R. Stevens, A review of growth mechanism, structure and crystallinity of anodized TiO2 nanotubes, Mater. Sci. Eng. R Reports. 74 (2013) 377–406. doi:10.1016/j.mser.2013.10.001.

[4] X. Chen, S.S. Mao, Titanium dioxide nanomaterials: Synthesis, properties, modifications and applications, Chem. Rev. 107 (2007) 2891–2959. doi:10.1021/cr0500535.

[5] P. Hartmann, D.K. Lee, B.M. Smarsly, J. Janek, Mesoporous TiO_2: Comparison of classical sol-gel and nanoparticle based photoelectrodes for the water splitting reaction, ACS Nano. 4 (2010) 3147–3154. doi:10.1021/nn1004765.

[6] G.K. Mor, O.K. Varghese, M. Paulose, K. Shankar, C.A. Grimes, A review on highly ordered, vertically oriented TiO_2 nanotube arrays: Fabrication, material properties, and solar energy applications, Sol. Energy Mater. Sol. Cells. 90 (2006) 2011−2075. doi:10.1016/j.solmat.2006.04.007.

[7] M. Zhang, T. Chen, Y. Wang, Insights into TiO_2 polymorphs: Highly selective synthesis, phase transition, and their polymorph-dependent properties, RSC Adv. 7 (2017) 52755–52761. doi:10.1039/c7ra11515f.

[8] T. Luttrell, S. Halpegamage, J. Tao, A. Kramer, E. Sutter, M. Batzill, Why is anatase a better photocatalyst than rutile? - Model studies on epitaxial TiO_2 films, Sci. Rep. 4 (2015). doi:10.1038/srep04043.

[9] Y. Luo, A. Benali, L. Shulenburger, J.T. Krogel, O. Heinonen, P.R.C. Kent, Phase stability of TiO_2 polymorphs from diffusion Quantum Monte Carlo, New J. Phys. 18 (2016) 113049. doi:10.1088/1367-2630/18/11/113049.

[10] D. He, H. Su, X. Li, H. Yu, M. Zubair, L. Wang, S. Mao, J. Wang, Heterostructure TiO_2 polymorphs design and structure adjustment for photocatalysis, Sci. Bull. 63 (2018) 314–321. doi:10.1016/j.scib.2018.02.008.

[11] W.-J. Ong, L.-L. Tan, S.-P. Chai, S.-T. Yong, A.R. Mohamed, Highly reactive {001} facets of TiO_2-based composites: synthesis, formation mechanism and characterization, Nanoscale. 6 (2014) 1946–2008. doi: 10.1039/c3nr04655a.

[12] X.Q. Gong, A. Selloni, Reactivity of anatase TiO_2 nanoparticles: The role of the minority (001) surface, J. Phys. Chem. B Lett. 109 (2005) 19560–19562. doi:10.1021/jp055311g.

[13] X. Kang, Y. Han, X. Song, Z. Tan, A facile photoassisted route to synthesis N, F-codoped oxygen-deficient TiO_2 with enhanced photocatalytic performance under visible light irradiation, Appl. Surf. Sci. 434 (2018) 725−734. doi:10.1016/j.apsusc.2017.10.226.

[14] J. Yu, Y.L. Yang, R.Q. Fan, L. Li, L.G. Wei, Mechanism of performance enhancement via fluorine doped titanium dioxide nanoparticles in dye sensitized solar cells, J. Fluorine Chem. 176 (2015) 71–77. doi:10.1016/j.jfluchem.2015.05.015.

[15] J. Low, B. Cheng, J. Yu, Surface modification and enhanced photocatalytic CO_2 reduction performance of TiO_2: a review, Appl. Surf. Sci. 392 (2017) 658–686. doi:10.1016/j.apsusc.2016.09.093.

[16] F. Xing, Q. Liu, M. Song, C. Huang, Fluorine Modified Boron Carbon Nitride Semiconductors for Improved Photocatalytic CO_2 Reduction under Visible Light, ChemCatChem. 10 (2018) 5270−5279. doi:10.1002/cctc.201801418.

[17] E.M. Samsudin, S.B. Abd Hamid, Effect of band gap engineering in anionic-doped TiO_2 photocatalyst, Appl. Surf. Sci. 391 (2017) 326–336. doi:10.1016/j.apsusc.2016.07.007.

[18] E. Ovodok, H. Maltanava, S. Poznyak, M. Ivanovskaya, A. Kudlash, N. Scharnagl, J. Tedim, Sol-gel template synthesis of mesoporous carbon-doped TiO_2 with photocatalytic activity under visible light, in: Mater. Today Proc., 2018: pp. 17422-17430. doi:10.1016/j.matpr.2018.06.044.

[19] M. Ge, C. Cao, J. Huang, S. Li, Z. Chen, K.-Q. Zhang, S.S. Al-deyab, Y. Lai, A Review of One-dimensional TiO_2 Nanostructured Materials for Environmental and Energy Applications, J. Mater. Chem. A. 4 (2016) 6772–6801. doi:10.1039/C5TA09323F.

[20] M. Abdullah, S.K. Kamarudin, Titanium dioxide nanotubes (TNT) in energy and environmental applications: An overview, Renew. Sustain. Energy Rev. 76 (2017) 212–225. doi:10.1016/j.rser.2017.01.057.

[21] K. Lee, A. Mazare, P. Schmuki, One-dimensional titanium dioxide nanomaterials: Nanotubes, Chem. Rev. 114 (2014) 9385–9454. doi:10.1021/cr500061m.

[22] N. Liu, X. Chen, J. Zhang, J.W. Schwank, A review on TiO_2-based nanotubes synthesized via hydrothermal method: Formation mechanism, structure modification, and photocatalytic applications, Catal. Today. 225 (2014) 34–51. doi:10.1016/j.cattod.2013.10.090.

[23] T.-S. Kang, A.P. Smith, B.E. Taylor, M.F. Durstock, Fabrication of Highly-Ordered TiO_2 Nanotube Arrays and Their Use in Dye-Sensitized Solar Cells, Nano Lett. 9 (2009) 601–606. doi:10.1021/nl802818d.

[24] R. Beranek, H. Hildebrand, P. Schmuki, Self-Organized Porous Titanium Oxide Prepared in H_2SO_4/HF Electrolytes, Electrochem. Solid-State Lett. 6 (2003) B12−B14. doi: 10.1149/1.1545192

[25] V. Zwilling, E. Darque-Ceretti, A. Boutry-Forveille, D. David, M.Y. Perrin, M. Aucouturier, Structure and Physicochemistry of Anodic Oxide Films on Titanium and TA6V Alloy, Surf. Interface Anal. 27 (1999) 629–637. doi:10.1002/(SICI)1096-9918(199907)27:7<629::AID-SIA551>3.0.CO;2-0.

[26] A. Ghicov, P. Schmuki, Self-ordering electrochemistry: A review on growth and functionality of TiO_2 nanotubes and other self-aligned MO_x structures, Chem. Commun. (2009) 2791–2808. doi:10.1039/b822726h.

[27] J.M. Macak, H. Tsuchiya, L. Taveira, S. Aldabergerova, P. Schmuki, Smooth anodic TiO_2 nanotubes, Angew. Chem. Int. Ed. 44 (2005) 7463−7465. doi:10.1002/anie.200502781.

[28] G.K. Mor, K. Shankar, M. Paulose, O.K. Varghese, C.A. Grimes, Enhanced photocleavage of water using titania nanotube arrays, Nano Lett. 5 (2005) 191–195. doi:10.1021/nl048301k.

[29] A. Valota, D.J. LeClere, P. Skeldon, M. Curioni, T. Hashimoto, S. Berger, J. Kunze, P. Schmuki, G.E. Thompson, Influence of water content on nanotubular anodic titania formed in fluoride/glycerol electrolytes, Electrochim. Acta. 54 (2009) 4321–4327. doi:10.1016/j.electacta.2009.02.098.

[30] D. Kowalski, D. Kim, P. Schmuki, TiO_2 nanotubes, nanochannels and mesosponge: Self-organized formation and applications, Nano Today. 8 (2013) 235–264. doi:10.1016/j.nantod.2013.04.010.

[31] R. Beranek, H. Tsuchiya, T. Sugishima, J. M. Macak, L. Taveira, S. Fujimoto, H. Kisch, P. Schmuki, Enhancement and limits of the photoelectrochemical response from anodic TiO_2 nanotubes, Appl. Phys. Lett. 87 (2005) 243114. doi:10.1063/1.2140085.

[32] L. Yang, M. Zhang, S. Shi, J. Lv, X. Song, G. He, Z. Sun, Effect of annealing temperature on wettability of TiO_2 nanotube array films, Nanoscale Res. Lett. 9 (2014) 621. doi:10.1186/1556-276X-9-621.

[33] S.P. Albu, A. Ghicov, S. Aldabergenova, P. Drechsel, D. LeClere, G.E. Thompson, J.M. Macak, P. Schmuki, Formation of double-walled TiO_2 nanotubes and robust anatase membranes, Adv. Mater. 20 (2008) 4135–4139. doi:10.1002/adma.200801189.

[34] E. Barborini, A.M. Conti, I. Kholmanov, P. Piseri, A. Podesta, P. Milani, C. Cepek, O. Sakho, R. Macovez, M. Sancrotti, Nanostructured TiO_2 films with 2 eV optical gaps, Adv. Mater. 17 (2005) 1842–1846. doi:10.1002/adma.200401169.

[35] R. Hahn, A. Ghicov, J. Salonen, V.P. Lehto, P. Schmuki, Carbon doping of self-organized TiO_2 nanotube layers by thermal acetylene treatment, Nanotechnology. 18 (2007) 105604. doi:10.1088/0957-4484/18/10/105604.

[36] J.H. Park, S. Kim, A.J. Bard, Novel Carbon-Doped TiO_2 Nanotube Arrays with High Aspect Ratios for Efficient Solar Water Splitting, Nano Lett. 6 (2006) 24–28. doi:10.1021/nl051807y.

[37] Y. Alivov, Z.Y. Fan, A method for fabrication of pyramid-shaped TiO_2 nanoparticles with a high {001} facet percentage, J. Phys. Chem. C. 113 (2009) 12954–12957. doi:10.1021/jp905174x.

[38] Y. Alivov, Z.Y. Fan, A TiO_2 nanostructure transformation: From ordered nanotubes to nanoparticles, Nanotechnology. 20 (2009) 405610. doi:10.1088/0957-4484/20/40/405610.

[39] H.G. Yang, C.H. Sun, S.Z. Qiao, J. Zou, G. Liu, S.C. Smith, H.M. Cheng, G.Q. Lu, Anatase TiO_2 single crystals with a large percentage of reactive facets, Nature. 453 (2008) 638–641. doi:10.1038/nature06964.

[40] R. Mohammadpour, A. Iraji zad, A. Hagfeldt, G. Boschloo, Investigation on the dynamics of electron transport and recombination in TiO_2 nanotube/nanoparticle composite electrodes for dye-sensitized solar cells, Phys. Chem. Chem. Phys. 13 (2011) 21487-21491. doi: 10.1039/c1cp21517e.

[41] D. Li, H. Haneda, S. Hishita, N. Ohashi, N.K. Labhsetwar, Fluorine-doped TiO_2 powders prepared by spray pyrolysis and their improved photocatalytic activity for decomposition of gas-phase acetaldehyde, J. Fluorine Chem. 126 (2005) 69–77. doi:10.1016/j.jfluchem.2004.10.044.

[42] X. Zhang, J. Zhang, H. Cui Adsorption mechanism of SF_6 decomposition components onto N, F-co-doped TiO_2: A DFT study, J. Fluorine Chem. 213 (2018) 18–23. doi:10.1016/j.jfluchem.2018.05.014.

[43] M. Fittipaldi, V. Gombac, A. Gasparotto, C. Deiana, G. Adami, D. Barreca, T. Montini, G. Martra, D. Gatteschi, P. Fornasiero, Synergistic role of B and F dopants in promoting the photocatalytic activity of rutile TiO_2, ChemPhysChem. 12 (2011) 2221–2224. doi:10.1002/cphc.201100254.

[44] K.W. Park, K.S. Seol, Nb-TiO_2 supported Pt cathode catalyst for polymer electrolyte membrane fuel cells, Electrochem. Commun. 9 (2007) 2256–2260. doi:10.1016/j.elecom.2007.06.027.

[45] A. Bauer, K. Lee, C. Song, Y. Xie, J. Zhang, R. Hui, Pt nanoparticles deposited on TiO_2 based nanofibers: Electrochemical stability and oxygen reduction activity, J. Power Sources. 195 (2010) 3105–3110. doi:10.1016/j.jpowsour.2009.11.107.

[46] J.M. Macak, F. Schmidt-Stein, P. Schmuki, Efficient oxygen reduction on layers of ordered TiO_2 nanotubes loaded with Au nanoparticles, Electrochem. Commun. 9 (2007) 1783–1787. doi:10.1016/j.elecom.2007.04.002.

[47] H. Maltanava, S. Poznyak, M. Starykevich, M. Ivanovskaya, Electrocatalytic activity of Au nanoparticles onto TiO_2 nanotubular layers in oxygen electroreduction reaction: size and support effects, Electrochim. Acta. 222 (2016) 1013–1020. doi:10.1016/j.electacta.2016.11.070.

[48] C. Zhang, H. Yu, Y. Li, L. Fu, Y. Gao, W. Song, Z. Shao, B. Yi, Highly stable ternary tin–palladium–platinum catalysts supported on hydrogenated TiO_2 nanotube arrays for fuel cells, Nanoscale. 5 (2013) 6834–6841. doi:10.1039/c3nr01086d.

[49] A. Sacco, N. Garino, A. Lamberti, C.F. Pirri, M. Quaglio, Anodically-grown TiO_2 nanotubes: Effect of the crystallization on the catalytic activity toward the oxygen reduction reaction, Appl. Surf. Sci. 412 (2017) 447−454. doi:10.1016/j.apsusc.2017.03.224.

[50] G.B. Harris, X. Quantitative measurement of preferred orientation in rolled uranium bars, London, Edinburgh, Dublin Philos. Mag. J. Sci. 43 (1952) 113–123. doi:10.1080/14786440108520972.

[51] C.S. Barrett, T.B. Massalski, Structure of Metals, Pergamon, Oxford, 1980.

[52] D. Bersani, G. Antonioli, P.P. Lottici, T. Lopez, Raman study of nanosized titania prepared by sol-gel route, J. Non. Cryst. Solids. 232–234 (1998) 175–181. doi:10.1016/S0022-3093(98)00489-X.

[53] F. Tian, Y. Zhang, J. Zhang, C. Pan, Raman spectroscopy: A new approach to measure the percentage of anatase TiO_2 exposed (001) facets, J. Phys. Chem. C. 116 (2012) 7515–7519. doi:10.1021/jp301256h.

[54] Y. Lai, L. Sun, Y. Chen, H. Zhuang, C. Lin, J.W. Chin, Effects of the Structure of TiO_2 Nanotube Array on Ti Substrate on Its Photocatalytic Activity, J. Electrochem. Soc. 153 (2006) D123−D127. doi:10.1149/1.2203112.

[55] B.M. Reddy, K.N. Rao, G.K. Reddy, P. Bharali, Characterization and catalytic activity of V_2O_5/Al_2O_3-TiO_2 for selective oxidation of 4-methylanisole, J. Mol. Cat. A: Chemical, 253 (2006) 44–51. doi:10.1016/j.molcata.2006.03.016.

[56] D. Gonbeau, C. Guimon, G. Pfister-Guillouzo, A. Levasseur, G. Meunier, R. Dormoy, XPS study of thin films of titanium oxysulfides, Surf. Sci. 254 (1991) 81–89. doi:10.1016/0039-6028 (91) 90640-E.

[57] J. Qiu, G. Zeng, M. Ge, S. Arab, M. Mecklenburg, B. Hou, C. Shen, A. V. Benderskii, S.B. Cronin, Correlation of Ti^{3+} states with photocatalytic enhancement in $_{TiO2}$-passivated p-GaAs, J. Catal. 337 (2016) 133–137. doi:10.1016/j.jcat.2016.02.002.

[58] B. Bharti, S. Kumar, H.N. Lee, R. Kumar, Formation of oxygen vacancies and Ti^{3+} state in TiO_2 thin film and enhanced optical properties by air plasma treatment, Sci. Rep. 6 (2016). doi:10.1038/srep32355.

[59] J.F. Moulder, W.F. Stickle, P.E. Sobol, K.D. Bomben, Handbook of X-ray Photoelectron Spectroscopy, Perkin Elmer Corp., Eden Prairie, MN, 1992.

[60] C. Yu, Q. Fan, Y. Xie, J. Chen, Q. shu, J.C. Yu, Sonochemical fabrication of novel square-shaped F doped TiO_2 nanocrystals with enhanced performance in photocatalytic degradation of phenol, J. Hazard. Mater. 237–238 (2012) 38–45. doi:10.1016/j.jhazmat.2012.07.072.

[61] J.C. Yu, J. Yu, W. Ho, Z. Jiang, L. Zhang, Effects of F-doping on the photocatalytic activity and microstructures of nanocrystalline TiO_2 powders, Chem. Mater. 14 (2002) 3808–3816. doi:10.1021/cm020027c.

[62] A.M. Czoska, S. Livraghi, M. Chiesa, E. Giamello, S. Agnoli, G. Granozzi, E. Finazzi, C. Di Valentiny, G. Pacchioni, The nature of defects in fluorine-doped TiO_2, J. Phys. Chem. C. 112 (2008) 8951–8956. doi:10.1021/jp8004184.

[63] H. Park, W. Choi, Effects of TiO_2 Surface Fluorination on Photocatalytic Reactions and Photoelectrochemical Behaviors, J. Phys. Chem. B. 108 (2004) 4086–4093. doi:10.1021/jp036735i.

[64] D. Li, N. Ohashi, S. Hishita, T. Kolodiazhnyi, H. Haneda, Origin of visible-light-driven photocatalysis: A comparative study on N/F-doped and N-F-codoped TiO_2 powders by means of experimental characterizations and theoretical calculations, J. Solid State Chem. 178 (2005) 3293–3302. doi:10.1016/j.jssc.2005.08.008.

[65] M.-Y. Hsu, W.-C. Yang, H. Teng, J. Leu, Microstructure and Composition of TiO_2 Nanotube Arrays Fabricated with HF and NH_4F Electrolytes and Their Evolution during Annealing, J. Electrochem. Soc. 158 (2011) K81−K87. doi:10.1149/1.3533388.

[66] Q. Zhang, V. Celorrio, K. Bradley, F. Eisner, D. Cherns, W. Yan, D.J. Fermín, Density of deep trap states in oriented TiO_2 nanotube arrays, J. Phys. Chem. C. 118 (2014) 18207–18213. doi:10.1021/jp505091t.

[67] S. V. Mentus, Oxygen reduction on anodically formed titanium dioxide, Electrochim. Acta. 50 (2004) 27–32. doi:10.1016/j.electacta.2004.07.009.

[68] V.B. Baez, J.E. Graves, D. Pletcher, The reduction of oxygen on titanium oxide electrodes, J. Electroanal. Chem. 340 (1992) 273–286. doi:10.1016/0022-0728(92)80303-L

[69] B. Parkinson, F. Decker, J.F. Julião, M. Abramovich, H.C. Chagas, The reduction of molecular oxygen at single crystal rutile electrodes, Electrochim. Acta. 25 (1980) 521−525. doi: 10.1016/0013-4686(80)87051-4.

[70] D.N. Pei, L. Gong, A.Y. Zhang, X. Zhang, J.J. Chen, Y. Mu, H.Q. Yu, Defective titanium dioxide single crystals exposed by high-energy {001} facets for efficient oxygen reduction, Nat. Commun. 6 (2015) 68696. doi:10.1038/ncomms9696.

[71] T. Clark, D.C. Johnson, Activation of Titanium Electrodes for Voltammetric Detection of Oxygen and Hydrogen Peroxide in Alkaline Media, Electroanalysis. 9 (1997) 273–278. doi:10.1002/elan.1140090402.

Figure captions

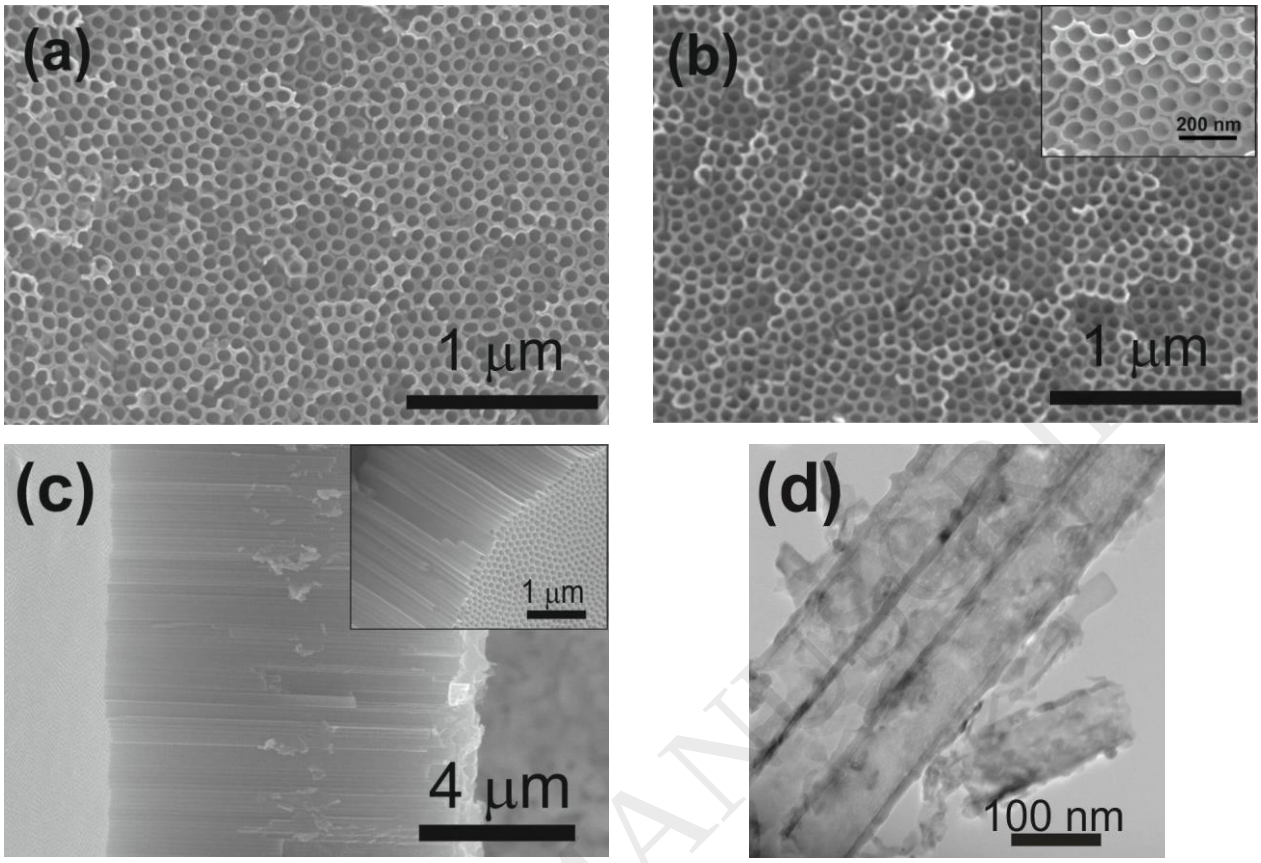

Figure 1. SEM top-view (*a*, *b*) and cross-section (*c*) images of the TiO_2 nanotubular layers before (*a*) and after annealing in air flow (*b, c*); TEM image of TiO_2 nanotubes after annealing in air flow (*d*). The insets show the magnified views of the corresponding samples.

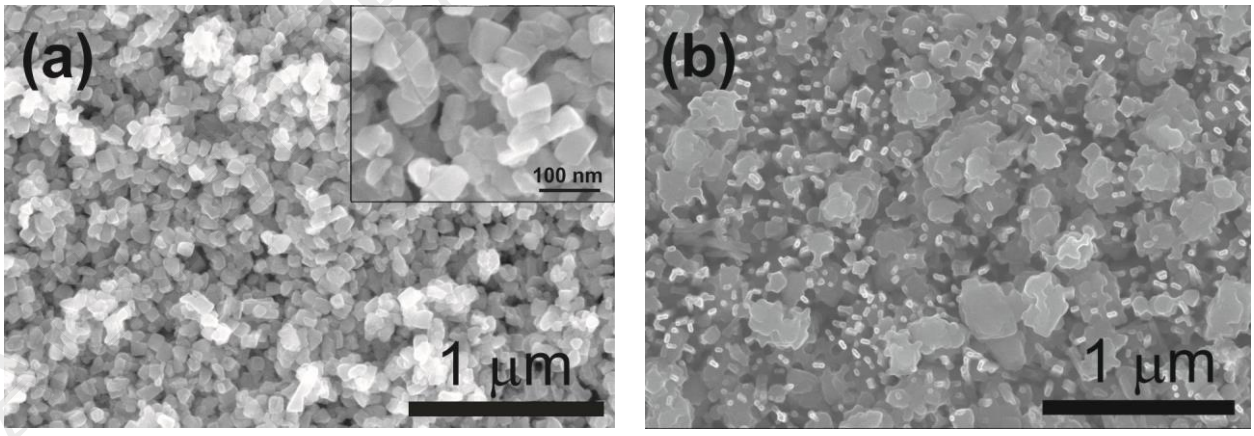

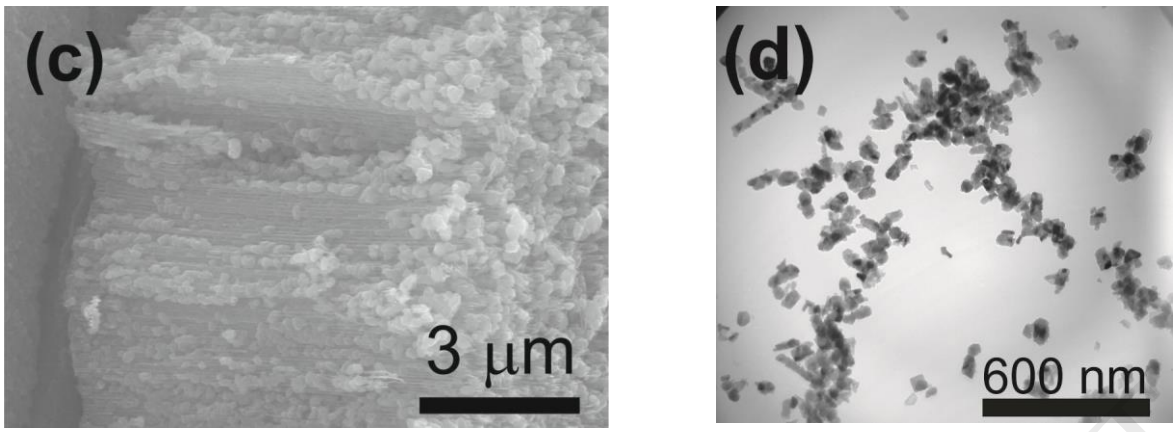

Figure 2. SEM top-view (*a*, *b*) and cross-section (*c*) images of the TiO_2 nanoparticulate layers, showing destruction of nanotubular structure at thermal treatment under limited air access conditions; TEM image of the TiO_2 nanoparticles (*d*). The inset shows magnified view of the corresponding sample.

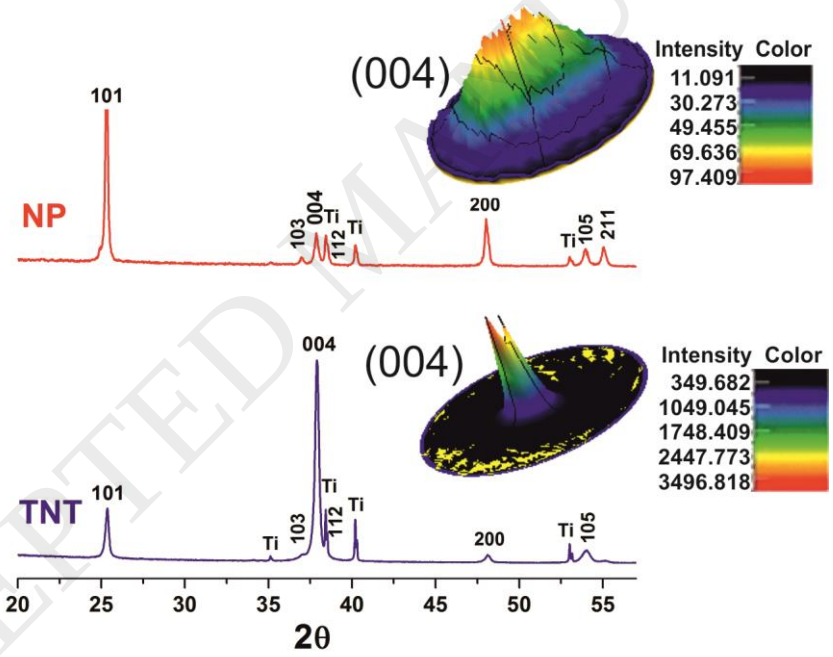

Figure 3. XRD patterns and the corresponding pole figures of the anatase TNT and NP samples. Notice the difference in scales of the pole figures.

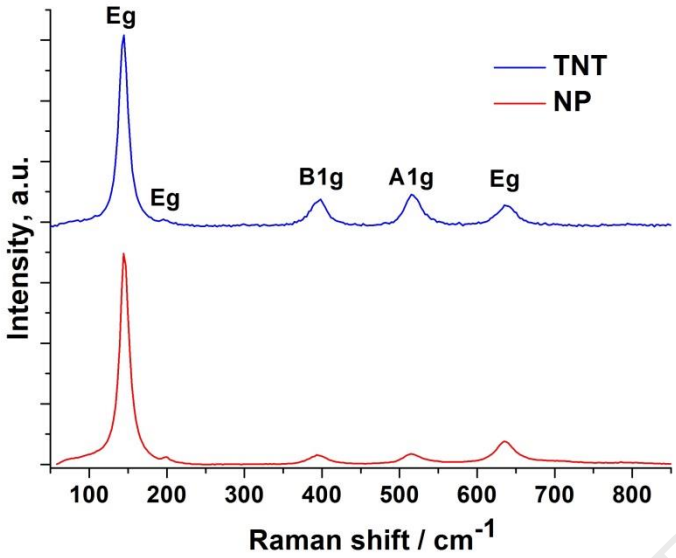

Figure 4. Raman spectra recorded in the 50 – 850 cm^{-1} range for annealed titania nanotubular (TNT) and nanoparticulate (NP) layers.

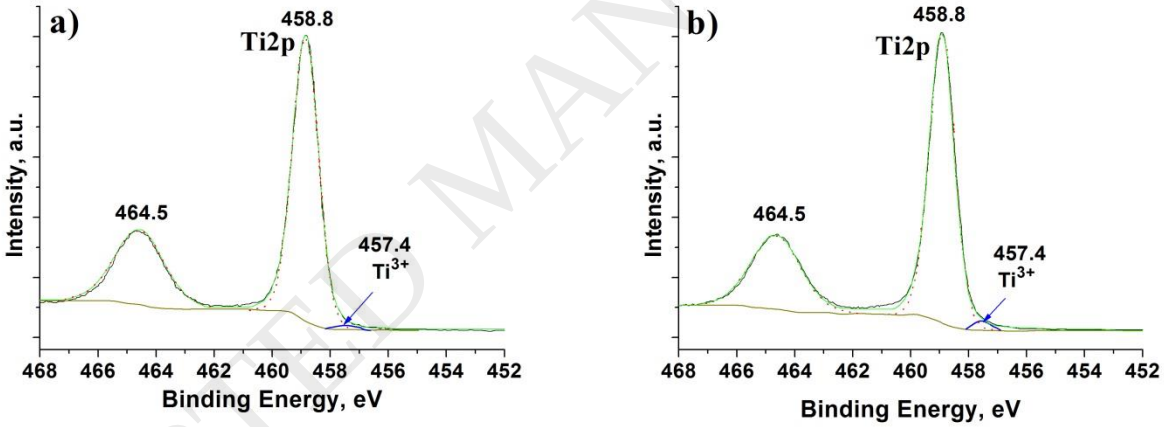

Figure 5. XPS spectra of the Ti 2p level for highly ordered TiO_2 nanotubular layers (*a*) and for TiO_2 nanoparticulate layers (*b*).

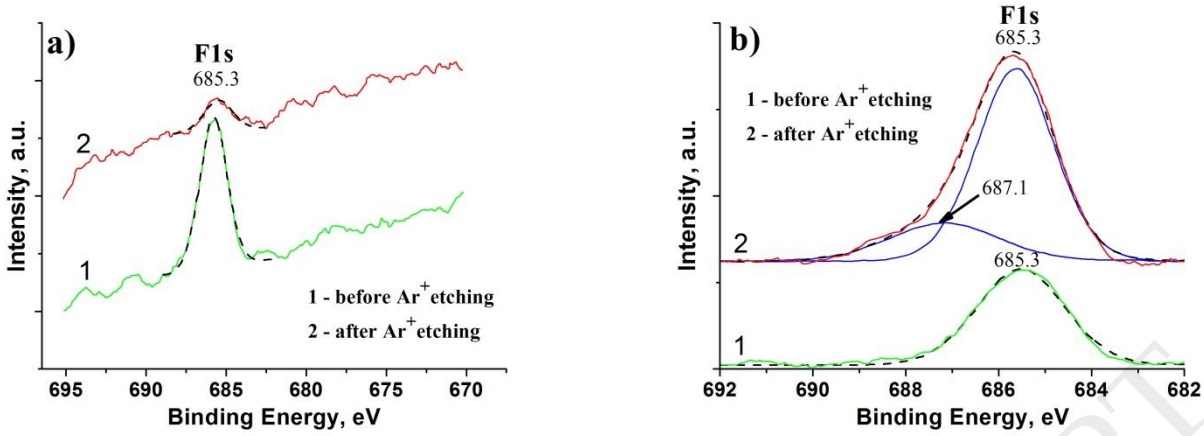

Figure 6. XPS spectra of the F 1s region for high-ordered TiO_2 nanotubular layers after annealing in air flow (*a*) and for TiO_2 nanoparticulate layers (*b*) formed as a result of annealing under limited air access conditions:

1– before Ar^+ etching; *2*– after Ar^+ etching.

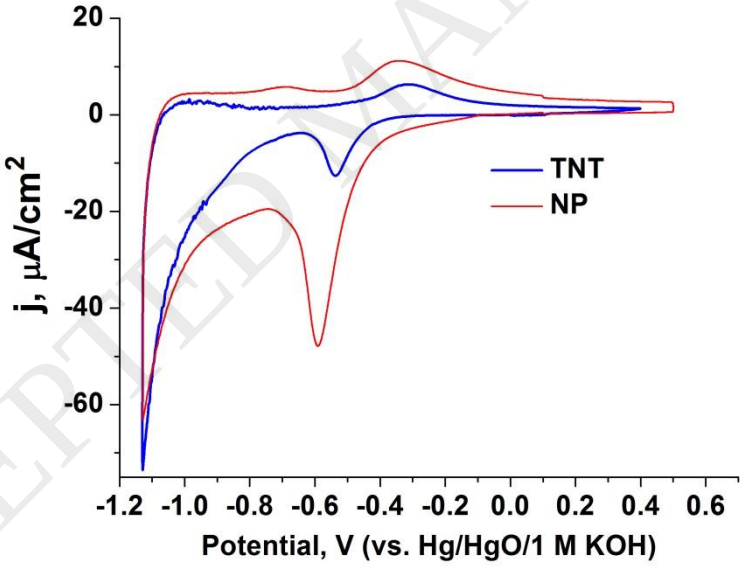

Figure 7. CV curves recorded in an Ar-saturated 0.1 M KOH solution for the TNT layers annealed in the air flow and for the NP layers thermally treated at limited air access. The potential scan rate was 10 mV/s.

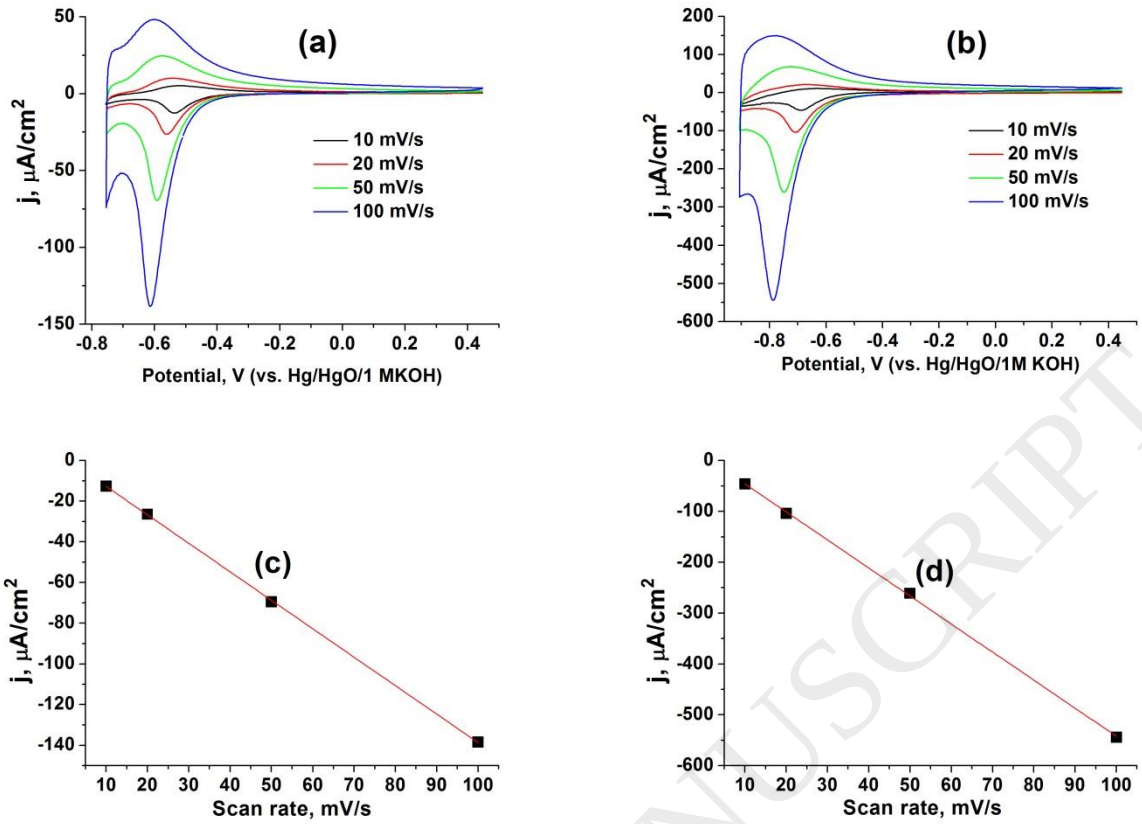

Figure 8. Cyclic voltammograms recorded at different potential scan rates on the TNT (a) and the NP (b) electrodes in an Ar-saturated 0.1 M KOH solution; the cathodic peak current as a function of the scan rate for the TNT (c) and the NP (d) electrodes.

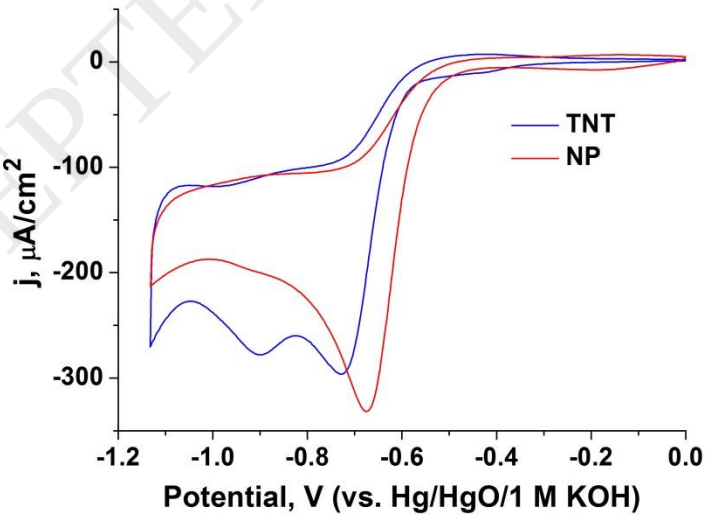

Figure 9. CV curves of ORR on the TNT and the NP electrodes in an oxygen-saturated 0.1 M KOH solution. The potential scan rate was 10 mV/s.